Preferential concentration and rise velocity reduction of bubbles immersed in a homogeneous and isotropic turbulent flow

A. Aliseda[1] and J. C. Lasheras[2]
[1]*Department of Mechanical Engineering, University of Washington, Seattle, Washington 98195, USA*
[2]*Department of Mechanical and Aerospace Engineering University of California, San Diego, California 92093, USA*

(Received 26 January 2011; accepted 5 July 2011; published online 6 September 2011)

The behavior of small spherical bubbles immersed in a homogeneous isotropic turbulent carrier flow of a heavier fluid has been experimentally studied. Air bubbles with diameters between 10 and 900 μm were injected in the test section of a horizontal water channel and allowed to interact with the turbulence induced by a grid located at the entrance to the test section. Point measurements of the bubble diameter and convective and rise velocities were taken from light interferometry data, together with flow visualizations that showed the instantaneous concentration field of bubbles in the carrier flow. The effect of the turbulence on the bubbles was found to alter the concentration field of bubbles leading to preferential accumulation at small scales, a phenomenon referred to as clustering, and to a decrease in the rise velocity of bubbles in the flow below the value measured and predicted for bubbles in a stationary fluid. These results are interpreted in terms of the different forces acting on the bubble in an inhomogeneous flow and in particular as the effect of pressure fluctuations that drive the bubbles preferentially to the core of vortices. © *2011 American Institute of Physics*. [doi:10.1063/1.3626404]

I. INTRODUCTION

The motion of bubbles immersed in a turbulent carrier flow is a basic problem in turbulent multiphase flows. An improved understanding of the dynamics of bubbles in turbulent flows as well as of the effect of their presence in the dynamics of the turbulence will lead to key advances in the fundamental modeling and predictive capabilities of multiphase systems. The design of heterogeneous chemical reactors where a reactant in the gas phase is bubbled through another in the liquid phase or the modelling of gas exchange between the ocean and the atmosphere are just two examples where a quantitative understanding of the physical phenomena that determines the interfacial surface area, slip velocity between the two phases, and residence time of the bubbles in the liquid is of fundamental importance. In these situations, the behavior of the bubbles is greatly influenced by the characteristics of the turbulence in the liquid phase. Thus, a well controlled laboratory experiment can produce valuable information on the effect of the underlying turbulence on the behavior of very small bubbles and, from the results, the different effects can be isolated and modeled to help predict the incidence of the various phenomena of interest in industrial and environmental applications.

The equation of motion for a rigid sphere, in the limit of zero particle Reynolds number, in a nonuniform flow has been established for several decades.[1] The applicability of this equation to bubbles in a turbulent liquid flow is, however, a matter of controversy. In common applications, such as air bubbles in water, bubbles with Stokes number of order one typically do not satisfy the conditions that the Reynolds number and the ratio of the diameter to the Kolmogorov length scale, η, are smaller than unity. The adequate treatment of hydrodynamic forces acting on a gas bubble under realistic conditions of Reynolds number and diameter to Kolmogorov microscale ratio is presented in a recent review by Magnaudet and Eames.[2] The adequate modeling of drag, added mass, shear-induced lift, and Basset force are all of importance in the trajectory of finite Reynolds number bubbles, where the relative magnitude of these forces needs to be carefully assessed.

The behavior of bubbles in flows dominated by the presence of large vortices has been the subject of in depth analytical and numerical[3,4] studies. These studies reported a preferential accumulation of bubbles in regions of high vorticity, confirming the intuition that microbubbles would be subject to the same accumulation effect due to turbulence that had been found for heavy particles.[5,6] In contrast to what happens with heavy particles, however, it was found that bubbles have their rise velocity reduced by the turbulence due to the increased residence time of the bubbles in the downward side of the eddies, where there is a theoretical static equilibrium point.[3] This is due to the fact that, instead of being driven by inertia to the downward convergence zones between eddies, they are driven to the eddies cores, where pressure forces oppose the buoyant rise that would take them away from these regions. A cartoon of this mechanism is drawn in Figure 1. Spelt and Biesheuvel[7] and Maxey[8] found these effects in their simulations of homogeneous isotropic turbulence laden with bubbles. Direct numerical simulations of bubbly turbulent flows have been performed by Druzhinin and Elgobashi,[9] who found that preferential accumulation is not significant for very small bubbles in low Reynolds number homogeneous, isotropic, decaying turbulence. Under these circumstances, the effect of the bubbles is similar to stratification, enhancing the turbulence decay for stable stratification and delaying it in the unstable case. Mazzitelli[10] reported the results of a DNS

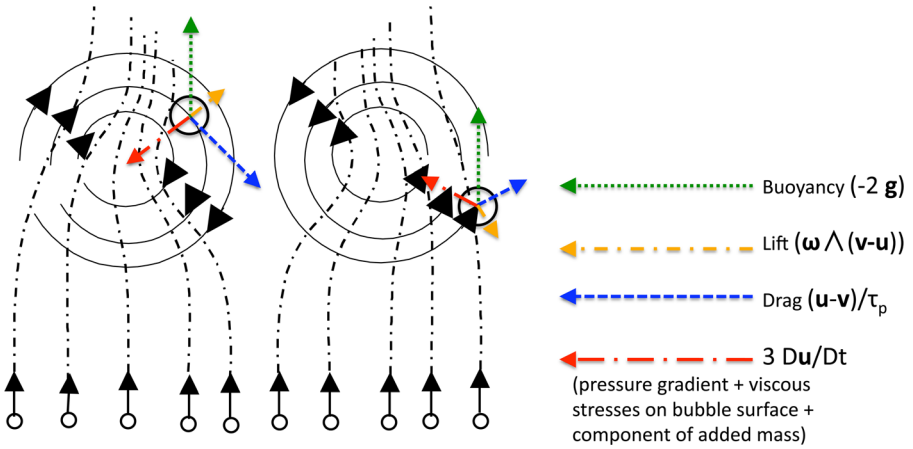

FIG. 1. (Color online) Rising bubbles interacting with a vortex pair. The bubble on the left is at the equilibrium point, where all forces are balanced resulting in zero velocity and acceleration. The bubble on the right is at a location where the acceleration, associated with added mass, is the result of the imbalance among buoyancy, drag, lift, and the term 3Du/Dt, which includes part of the added mass term and the pressure and viscous stresses on the surface of the bubble due to the non uniform flow (not included in the drag force).

study of microbubbles in homogeneous isotropic turbulence. They focused the attention on the effect of lift force and found that bubbles increase their residence time in the downward side of the eddies, thus reducing the bubble mean rise velocity. Large scale velocity fluctuations in the carrier fluid are inhibited by the buoyancy, while energy is added at the small scales of the turbulence, resulting in a net reduction of the turbulence decay rate. Numerical simulation of small bubbles dispersed in shear flows[11,12] has shown that bubble dispersion is dominated by the interaction of buoyancy with the complex hydrodynamic forces that develop in the neighborhood of large coherent vortices, including drag, added mass, and lift. The presence of equilibrium points near the vortex cores, a phenomenon that depends on the bubble Stokes number, dominates the residence time of bubbles in the vortical region of the flow,[11,13] as well as the two-way coupling effect of bubbles on the vorticity field.[12]

The experimental study of turbulent bubbly flows has been mostly carried out with relatively large bubbles and volume fractions. In their seminal paper, Lance and Bataille[14] studied the turbulence characteristics of the continuous phase in an upwards flowing water channel, where turbulence was introduced both by a grid and by ellipsoidal bubbles with an equivalent diameter of 5 mm, approximately equal to the Taylor microscale of the single phase flow. As the bubble void fraction was increased from 0% to 5%, they found that the flow transitioned from a regime, where the hydrodynamic interaction of the bubbles is negligible to one in which the bubbles transfer a great amount of kinetic energy to the flow, modifying the one dimensional spectra from the classical $-5/3$ power law to a $-8/3$ dependency. More recently, the problem of bubbles injected into an upward-moving, grid-induced turbulent water flow was revisited, and the bubble spatial distribution as well as the effect of the bubbles on the underlying carrier flow turbulence were characterized.[15] A non uniform distribution of bubbles was found, with a peak in the local void fraction located approximately halfway between the channel wall and the centerline. An associated peak in the streamwise velocity was also reported, presumably induced by the stronger buoyancy of the bubbles at the location of the void fraction peak. The reasons for the existence of these peaks and their location were not provided, and several mechanisms, such as lift due to the interaction with the mean shear[16] or preferential accumulation by large eddies,[17] were suggested as possible causes. Because in these experiments the bubbles were several millimeters in diameter and the volume fraction was high ($\approx$5%), the effect of the carrier flow on the dynamics of the bubbles was masked by other stronger effects. Moreover, because the mean flow was in the same direction as gravity, the rise velocity was not considered. Experiments to determine the forces acting on bubbles in the 500-800 μm range due to nonuniform flow were conducted by Sridhar and Katz.[18] They found drag coefficients that agreed well with steady state data and lift coefficients that did not agree with existing theoretical or numerical models. In the course of their experiments, they measured the trajectory of a bubble entrained by a laminar vortex and were able to reproduce it with calculations using the equation of motion described above[2] with adequate coefficients. The dispersion of microbubbles in a free shear layer has been studied using bubbles with diameters smaller than 100 μm.[17] In this case, the rise velocity of the bubbles was negligible, but the experiment was able to characterize the effect of the large coherent vortices present in a mixing layer on bubble dispersion. The dispersion of larger, millimeter-scale, bubbles in turbulent mixing layers is dominated by a combination of buoyancy and hydrodynamic forces[19,20] with a complex feedback mechanism, whereby the bubbles contribute significantly to the velocity fluctuations and, therefore, to the mixing spreading rate through pseudo-turbulence associated with added mass and the relative high Reynolds number in their wakes. More recently, experimental evidence of a decrease in the rise velocity of bubbles caused by homogeneous isotropic turbulence which is created by an active grid has been reported.[21] These experiments have established experimentally, for the first time, the predicted reduction in the rise velocity of bubbles below the value measured in still fluid, due to the effect of homogeneous isotropic turbulence.

In this paper, we present recent experimental evidence of turbulence-induced reduction of the rise velocity of

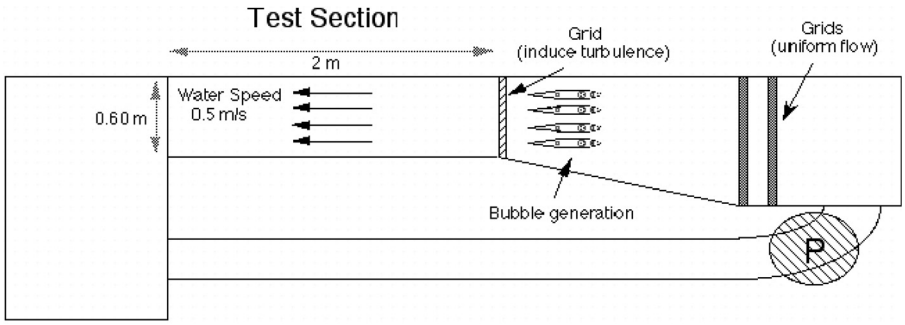

FIG. 2. Recirculating water channel.

bubbles under a wide range of values of the controlling parameters. The bubble Stokes number, the bubble void fraction, and the carrier flow turbulent intensity have been systematically varied in the range of interest, namely dilute concentration of bubbles and diameters smaller or equal than the Kolmogorov microscale. We also extend the analysis of this phenomenon with experimental evidence and quantitative measurements of preferential concentration of microbubbles in homogeneous isotropic turbulence. The structure of the paper is as follows: the experimental setup is described in Sec. II, the measurements of the bubble rise velocity, as a function of the bubble diameter, void fraction, and turbulence intensity are reported in Sec. III. The relevant bubble rise velocity in still fluid, used for comparison with the measurements in a turbulent flow, as well as the scaling of the rise velocity reduction found in the experiments are analyzed in Sec. IV. Finally, the conclusions reached in the study are summarized in Sec. V.

II. EXPERIMENTAL METHODS

A. Experimental facility

The experiments were carried out in a recirculating water channel with a capacity of roughly 5 cubic meters. The test section is 2 m long and has a square cross section of 0.6 m $\times$ 0.6 m. The maximum free stream velocity in the test section is 1 m/s. A sketch of the facility is shown in Figure 2. The facility has a series of grids and honeycombs, followed by a 3:1 area-ratio contraction, to ensure that fluctuations originating at the pump are damped out before the flow reaches the test section. The underlying turbulent intensity in the original channel flow is very low, less than 0.5%, and the homogeneous isotropic turbulence is generated by a grid located at the entrance to the test section. The grid was formed by cylindrical bars with a diameter of 0.3175 cm and a spacing of 2.54 cm, which gives a solidity ratio of 0.11. At different mean velocities of the carrier flow, the grid induces different levels of turbulent fluctuations, enabling us to study the behavior of the bubbles under varying conditions of the turbulence. The experimental conditions are shown in Table I.

The bubbles were introduced in the flow by an array of thin hydrofoils located a small distance in front of the turbulence-inducing grid. They were positioned horizontally and arranged in a grid type structure, separated 10.16 cm from each other and from the top and bottom of the channel, so the perturbation due to the bubble injecting device was just a small contribution to the overall turbulence. The injectors were embedded in the hydrofoils to minimize their wakes.

Each injector consists of an aluminum NACA 0012 profile with a longitudinal cavity machined along its leading edge. The cavity is closed with a porous plate through which compressed air, injected from the side of the hydrofoil, is bubbled into the incoming flow. The experiments required the injection of very small bubbles, $d_{30} \approx 200$ μm, in very large numbers so that the volume fraction would be significant to study accumulation effects, $\varphi \approx 10^{-4}$. To reduce the bubble size, ethanol micro-jets are directed at the porous plate along the leading edge of the hydrofoil so that the contact angle of the growing bubbles is increased, making it easier for bubbles to detach from the plate. Essentially, as the volume to cross-sectional area ratio is decreased and since drag depends on the area exposed to the incoming fluid, bubbles with smaller volume are formed. A schematic of the device and the mechanism of size reduction are shown in Figure 3. The volume of alcohol injected during the experiment was very small, approximately 1 ml/s, and so its effect on the bulk properties of the carrier fluid was negligible.

B. Turbulence characterization

The turbulence was characterized with laser Doppler velocimetry. A Phase Doppler Particle Analyzer (PDPA) (TSI Inc., Lakeside, MN) was mounted on the water channel and collected light scattered from the bubbles flowing through the probe volume. A water-filled triangular prism was placed on the free surface to provide a clean optical path for the scattered light to reach the PDPA detector. The prism was designed to use internal reflection, which gives the highest efficiency and resolution in the diameter measurements (largest slope of phase-vs-diameter relationship), allowing

TABLE I. Experimental conditions in the water channel. Turbulence characteristics at the location of the measurements.

U_∞ (m/s)	u' (m/s)	Re_M	u'/U_∞ (%)	u'/w'	ϵ (m^2/s^3)	τ_k (10^{-3} s)	η (10^{-6} m)	v_k (10^{-3} m/s)
0.40	0.10	10 000	25	1.10	0.005	14	120	8.4
0.63	0.16	15 500	26	1.06	0.006	13	114	8.8

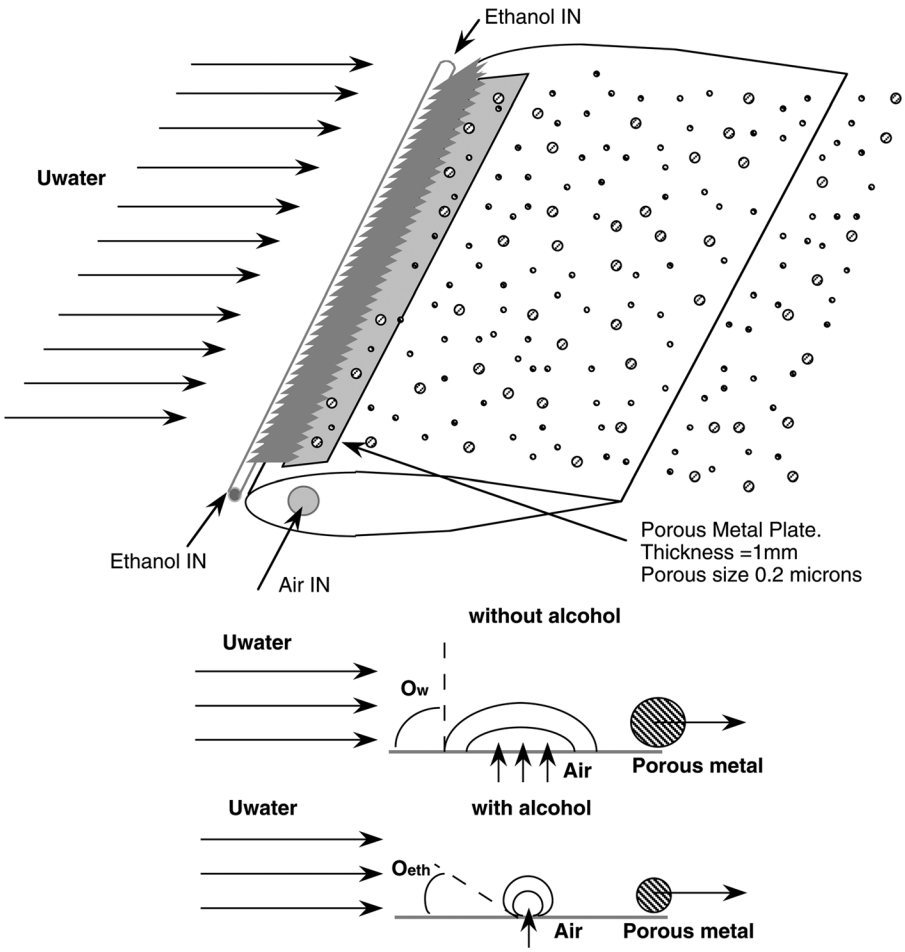

FIG. 3. Sketch of the bubbler and the diameter reduction mechanism.

the detector to be focused on the probe volume at an angle of 63° for forward scattering collection.[22] A sketch of the setup is shown in Figure 4. This system, which has been described at length elsewhere,[23] uses the frequency and phase shift of light reflected by the bubbles as they cross through the probe volume to compute their velocity and diameter. Briefly, two pairs of light beams with different wavelengths are projected into the test section, perpendicular to each other, and intersect at a certain point in the flow, materializing the probe volume. Because a small frequency shift has been introduced in one of the beams in each pair, they create an interference pattern, with fringes moving in two perpendicular directions when the beams cross inside the probe volume. Every bubble that crosses that volume reflects light modulated by the constructive-destructive interference in both wavelengths. The system acquires and analyzes the reflected light, computing the frequencies and phase shift introduced by the bubbles as they cross the fringes. From that information, the system calculates the diameter of the bubbles, based on Mie scattering theory, and two components of the velocity associated with the two directions of the fringe patterns, in this case the streamwise and vertical components. Using the smallest bubbles as flow tracers, the carrier fluid velocity components in two perpendicular directions, along the mean flow and along the direction of gravity, were obtained from the PDPA measurements by filtering out the data for bubbles larger than 50 μm. From these measurements, the turbulence characteristic length, time, and velocity scales were computed. The homogeneity and isotropy of the flow in planes perpendicular to the mean flow were also confirmed.

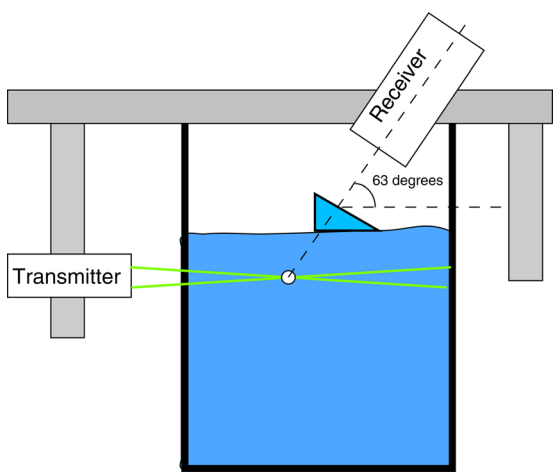

FIG. 4. (Color online) Sketch of the mount used to take PDPA measurements on the water channel. This view shows the cross section of the channel, perpendicular to the flow direction.

C. Bubble diagnostics

Flow visualizations were used to obtain information on the spatial distribution of the bubbles. This technique allowed a large area of the flow to be sampled. While the PDPA technique described above provided point

measurements that were analyzed over time to provide bubble statistics, flow visualizations gave instantaneous information on the distribution of bubbles in a large area in the flow. To obtain an instantaneous visualization of the position of the bubbles in the flow, a vertical slice of the flow was illuminated by a laser plane projected from the bottom of the test section. The beam from an Ar^+ laser (Innova 70C-5W, Coherent Inc., Santa Clara, CA) was redirected to a rotating mirror located under the test section of the channel. The light beam swept the flow at 4000 Hz, creating a vertical plane inside the channel. The light reflected by the bubbles was captured by a Kodak ES 1.0 digital high resolution (1008×1008 pixels) charged coupled device (CCD) camera with its focal axis located perpendicular to the laser plane. Using NIH IMAGEJ processing software, large sets of images taken with this method were made binary and analyzed, following a procedure that has produced excellent results in the past.[24] Following this image processing technique, the location of the bubble centroid was computed and stored. By analyzing a large number of images taken under the same conditions, statistics of the concentration field of the particles could be built and the influence of the turbulence studied. Information on the preferential accumulation of bubbles obtained with this method is presented in Sec. III C.

III. EXPERIMENTAL RESULTS

Four sets of experiments were conducted to study the influence of the carrier flow turbulence on the rise velocity and concentration field of the bubbles. The first one looked at the rise velocity of relatively large bubbles, in the range 300-900 μm, using PDPA measurements. The second used a point source of bubbles and measurements at different distances downstream and at different free stream velocities to evaluate the rise velocity of small bubbles (200-400 μm) with higher accuracy. The third one was similar to the first set of experiments but used modified PDPA optics and signal processing settings to look at the rise velocity of smaller bubbles, in the range 10-300 μm. Finally, flow visualizations were used to study the bubble instantaneous concentration fields under both conditions.

A. Large bubbles ($d = 300 - 900$ μm)

We measured the streamwise and vertical velocities of the bubbles within a wide diameter range ($d = 300 - 900$ μm), as well as their size, at two different locations downstream from the grid, $x/M = 24$ and $x/M = 30$, and at different mean velocities of the water channel. The rise velocity obtained by averaging the vertical velocities of all bubbles within each size range are plotted in Figure 5, as a function of the average diameter of the bubbles for each size bin. To measure in this large range of bubble diameters, there is a trade off in the PDPA settings between accuracy in the rise velocity measurements and sampling rate. Due to the low PDPA data rate in this regime and the uncertainty in the measurements of the vertical velocity, the smallest size class was chosen to include all bubbles with diameters between 0 and 250 μm. This wide range was necessary to ensure that a large enough number of bubbles were used to compute the

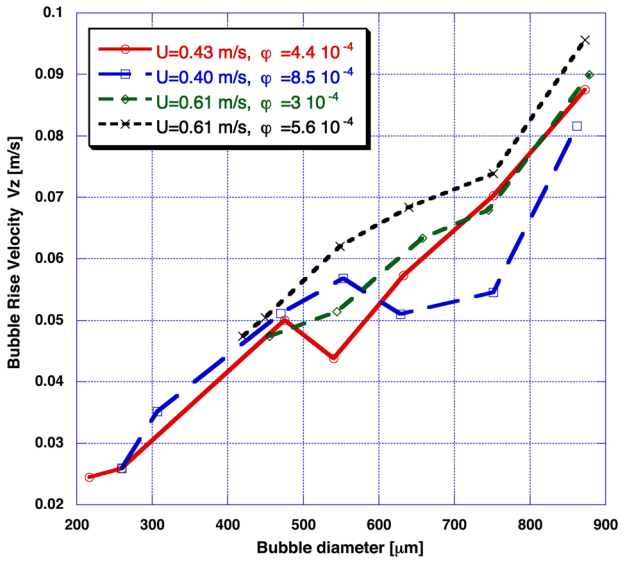

FIG. 5. (Color online) Measurements of the average vertical velocity of the bubbles.

statistics of the velocity. It was critical to obtain reliable statistics of the smaller size class, as they were used to characterize the turbulence, and more importantly, the mean vertical velocity of the smallest size class was used to align the laser beams to a horizontal axis. Misalignment between the laser beams and the horizontal axis of the channel would cause a small component of the streamwise velocity being measured as part of the vertical velocity, contaminating the data.[6] Thus, the laser beams were rotated in their mount until the mean vertical velocity of the smallest class was found to be zero within experimental error. This alignment of the PDPA measuring axis results in a small underestimation of the rise velocity of bubbles, associated with the assumption that the smallest bubbles have zero vertical velocity. To correct for this, the rise velocity of bubbles between 0 and 250 μm (within the smallest size range used in the PDPA) was computed by an indirect method explained below and added to the PDPA measurements. The resulting velocities have a systematic error related to the cosine in the projection that is proportional to $\alpha^2/2$, where α is the angle that the PDPA axis forms with the horizontal, $\alpha = \tan^{-1}(V_z^0/V_x)$. In the experiments, $V_z^0 \approx 2.5\ 10^{-2}$m/s and $V_x \approx 7.5\ 10^{-1}$ m/s, so the error is of the order of 1/1000 of the measurement, much smaller than the intrinsic accuracy of the PDPA. Figure 6 shows the same data, made non dimensional with the root mean square of the fluctuating velocity and plotted against the Stokes number of the bubbles. It can be observed that the data made non dimensional in this way show a consistent behavior over different values of the turbulence intensity and void fraction.

In order to improve the accuracy of the analysis, we developed a new technique to obtain measurements of the bubble rise velocity independent of the alignment of the PDPA laser beams. Specifically, we used this method to characterize the rise velocity of very small bubbles ($50 - 250$ μm). A single bubble injector was used to introduce a point source of bubbles in the flow. The size probability density function of bubbles was measured at two different locations

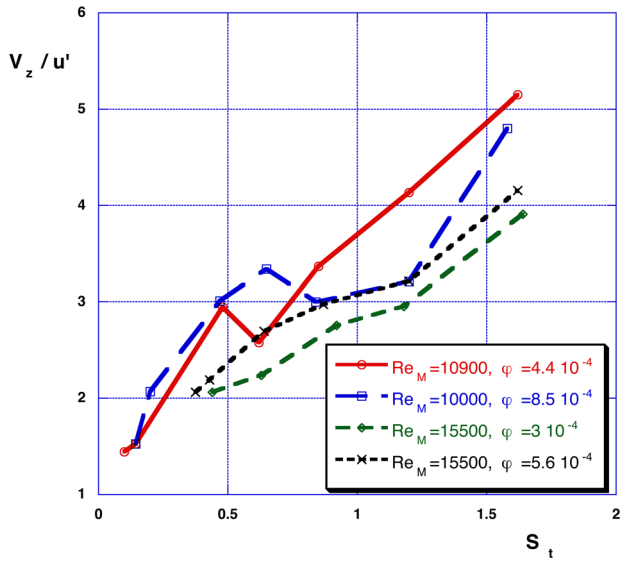

FIG. 6. (Color online) Normalized average rise velocity of the bubbles.

downstream (L), and a small distance above (H), from the source, and the turbulence inducing grid. The evolution of the bubble cloud under mean flow convection, turbulence dispersion, and buoyant rise would make the size distribution vary spatially, as sketched in Figure 7. Each class size of bubbles in the cloud ($d_i < d < d_{i+1}$) will follow a parabolic trajectory, on average, determined by their mean rise velocity and spreading due to turbulent dispersion. If one compares two size probability density functions measured at small distance apart, one would find that there is a bubble size for which the number of bubbles per unit time passing through the measurement point has not changed, whereas the number of bubbles for all sizes larger than that decreases (because they rise faster and the measurements are already in the tail of the distribution) and all sizes smaller than the unchanged one will increase their number (because they rise slower and they have not yet reached the maximum in the distribution). The size class that is going through the maximum at the location of the measurements has an average rise velocity that can be computed from geometrical considerations as $V_z = U_\infty \cdot H/L$. The result from this calculation is shown in Figure 8. From these measurements, we obtained a value of the rise velocity, independent of the laser alignment, that was used to correct the data plotted in Figure 5, thus canceling the subtraction of the rise velocity of the smallest bubbles introduced by the PDPA beam alignment method.

B. Small bubbles ($d = 10 - 400\ \mu$m)

To study the rise velocity of smaller bubbles, selecting a narrower diameter range allowed for better accuracy in the velocity measurements and higher sampling rate. Modifications to the laser optics as well as to the data acquisition settings were introduced to greatly increase the resolution with which the bubble vertical velocity could be measured by the PDPA. The rise velocity of the smallest bubbles was directly measured with a resolution better than 5×10^{-3} m/s, and the results are shown in Figure 9 for two values of the turbulent intensity. For comparison, the values of the rise velocity in still fluid predicted by three different correlations available in the literature are plotted in the same figure. The values of the rise velocity predicted for triply distilled water doped with a high concentration of a surfactant,[25] and for tap and sea water,[26] agree quite well. The uppermost curve is given by a simple Stokes law, without corrections for finite Reynolds number. It is important to point out that, even though the smallest bubbles in previous experiments[25,26] were larger than the ones reported here, they found the behavior of the bubbles to be very close to the rigid bubble with no internal

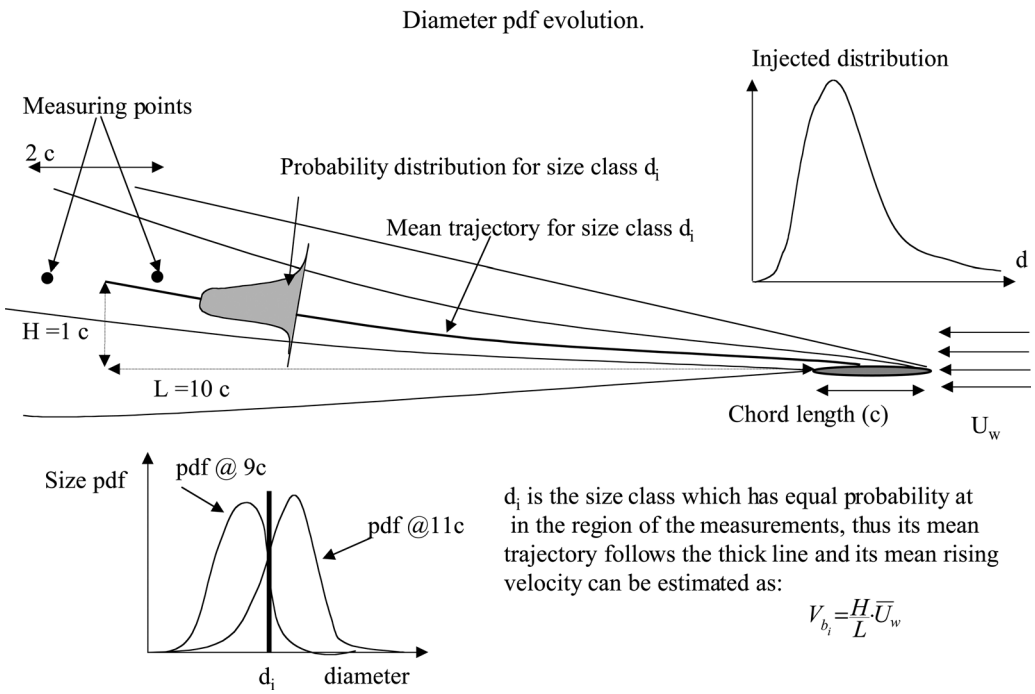

FIG. 7. Schematic of the vertical velocity measurement based on the evolution of the bubble size distribution.

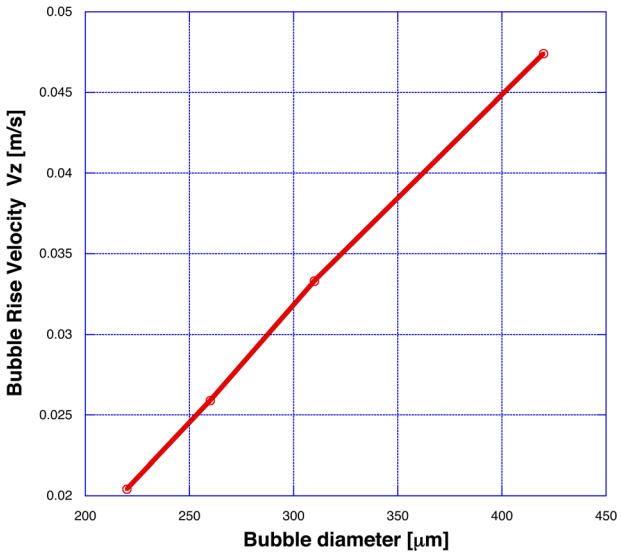

FIG. 8. (Color online) Indirect measurements of the average rise velocity for the smallest bubbles.

circulation.[27] Thus, for the bubbles in this range (10-300 μm), the clean, stress-free surface with internal circulation condition is considered irrelevant in water and other polar liquids (but would not be in non-polar carrier fluids) and only the correlations obtained for rigid bubbles loaded with surfactants have been considered. The measurements are still subject to the alignment problem, and so the system was again aligned until the smallest class size, in this case 5-50 μm, was found to have zero vertical velocity. It is important to note that, unlike in the previous case, the expected rise velocity of these bubbles is only a few millimeters per second, and thus the error introduced by the alignment method is smaller than the intrinsic accuracy of the measurements. The results agree well with the indirect measurements taken by the evolution of the size distribution, detailed above, and complement the measurements of the rise velocity of large bubbles explained in Sec. III A.

C. Bubble concentration field

The instantaneous concentration field of bubbles in the flow was investigated by analyzing visualizations of vertical slices of the flow illuminated by a laser plane. There are multiple methods that have been used to characterize the deviation of the instantaneous concentration of bubbles from randomness. We found that the method that provided the best results was the comparison of the actual statistics of bubbles locations in the flow, with the theoretical probability density function expected if the bubbles were randomly distributed by the turbulence.[5,28] The position of the bubbles was obtained by processing the images of the light scattered at 90° by the bubbles in the flow. The image plane was divided in square windows of a certain size and the number of bubbles in each window counted. The probability density function of the bubble concentration was computed by counting the number of bubbles per window, for all the windows of a certain size in all the images taken under the same flow conditions. This probability distribution was then compared to a Poisson distribution, which is the probability distribution corresponding to a random field of bubbles. To obtain a quantitative measure of the deviation from randomness, we used two parameters that have been widely used in the literature on preferential accumulation.[5,28] The first method compared the experimental and theoretical pdfs point by point ($P - P_{Poisson}$) and calculates a mean square distance between the two. In the second method, only the standard deviation of both experimental and theoretical pdfs is compared ($\sigma - \sigma_{\text{Poisson}}$) and made non dimensional with the mean value for the pdf (μ) that is common to both. If this algorithm is applied for varying sizes of the windows, the evolution of these parameters quantify the extend to which clustering occurs in this flow. The distributions obtained from very small windows, comparable to the smallest flow scales, must be very similar to the random distribution: since the process becomes binary, there is zero or one bubble in each window. For very large windows, larger than the integral length scale of the turbulence, the process again

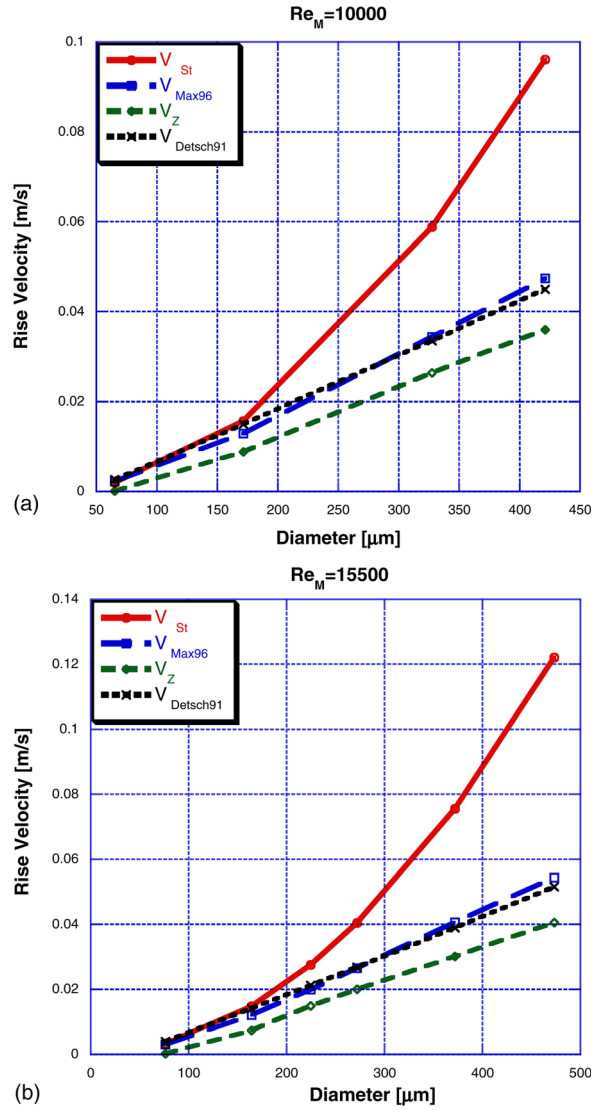

FIG. 9. (Color online) Direct measurements of the rise velocity for small bubbles (V_Z). Comparison with three different estimates of the rise velocity of small bubbles in still fluid. V_{St} is the theoretical rise velocity for a spherical gas bubble with $C_D = 24/Re$, V_{Max96} is the value obtained from experimental measurements in triply distilled water,[25] and $V_{Detsch89}$ is the value from experimental measurements in tap and salt water.[26]

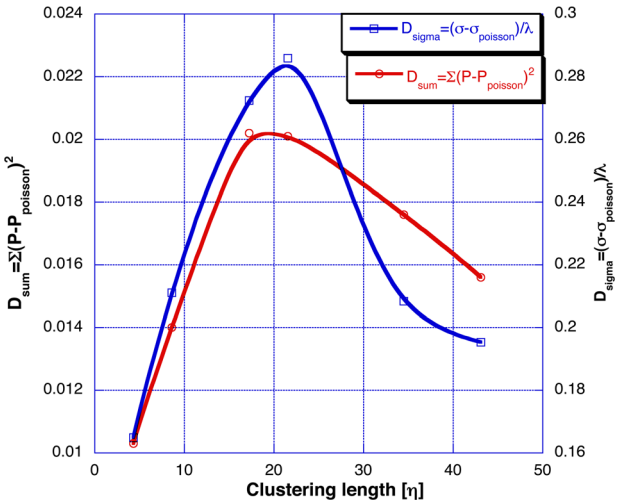

FIG. 10. (Color online) Preferential concentration of bubbles. Characteristic length scale. U = 0.25 m/s, $\alpha = 8 \times 10^{-4}$.

resembles a random distribution, as each window contains regions of high concentration and regions devoid of bubbles and the process of counting the bubbles integrates the concentration field, smearing the clusters. The results from this process can be seen in Figure 10, for a particular value of experimental settings. All experimental conditions were tested, and the results were consistent among all of them. As predicted by the theory, the deviation from randomness parameters showed the tendency to zero for both very large and very small window sizes, although the largest windows were not large enough to reach a zero value. At the intermediate scales, however, preferential accumulation of bubbles was present in every case, and it was maximum for windows with a size corresponding to about 20 times the Kolmogorov length scale. This is about twice the characteristic size of the particle clusters found in other experiments,[6] where the Reynolds number in the flow was lower (10^5 vs 6×10^5). This is consistent with the idea that clusters are formed by small scale vorticity and the peak of the dissipation spectrum moves to larger scales (lower wavenumbers) for larger Reynolds number flows.

IV. ANALYSIS

The effect of turbulence on the dynamics of bubbles is a problem rich in physics that is governed by at least four non dimensional parameters: the Stokes number ($St = \tau_b/\tau_k$) is the ratio of the bubble viscous response time to the Kolmogorov turn over time and characterizes the influence of the bubble inertia, as it accelerates the surrounding fluid it displaces in its trajectory. The terminal velocity ratio (V_t/V_k) is the ratio of the bubble rise velocity in still fluid to the Kolmogorov velocity, and it represents that influence of the crossing trajectories effect, due to the vertical velocity breaking the symmetry of the interaction of the bubbles with the turbulent fluctuations, on the bubble dynamics. The geometrical ratio of the bubble diameter to the Kolmogorov length scale (d/η) also influences the scale at which the bubbles sample the velocity fluctuations in the turbulence and the resulting shear. These three parameters do not vary independently of each other for a certain turbulent carrier flow and a certain gravity field. As such, only one of the values can be changed independently. For this analysis, we have chosen to evaluate the physics of the bubble-turbulence interactions in terms of the Stokes number, as the leading order effect in the bubble trajectories. The ratio of bubble diameter to Kolmogorov scale is of order one ($0.2 < d/\eta < 2$), which makes the results directly comparable to most DNS study, where the equation of motion used for the bubbles require this ratio to be smaller than one. The terminal velocity ratio can also be directly linked to the Stokes number for a given fluid and turbulence intensity ($V_t/V_k = \tau_p g \tau_k \nu^{3/4}/\epsilon^{1/4}$) and is also of order one for all the experiments presented here. The fourth non dimensional parameter of importance is the bubble void fraction. The range of void fraction under study is limited, from 4×10^{-4} – 8×10^{-4}, and no definite conclusions have been reached on its effect in these experiments. The results are, however, tagged with the value of φ so as to provide a reference for further studies of the mechanism by which the void fraction affects the bubble-turbulence dynamics.

To establish the effect of the turbulence on the rise velocity of the bubbles, one needs to compare the measured rise velocities with the values that those same bubbles would have in a stationary fluid. This is not a simple task, as the rise velocity of a bubble in still fluid is not simply determined by its diameter and relative density, as is the case with the settling of a spherical particle. There are different regimes depending on the surface tension between the fluids and the shape of the bubble. Bubble behavior can evolve continuously between that of a rigid sphere with no internal circulation and that of a fluid sphere with a free-stress boundary,[25] depending on the values of surface tension and the viscosity. They also go through different regimes: sphere, ellipsoid, and spherical cap as the size and Reynolds number increases.[27] The bubbles in these experiments keep their spherical shape, but it was not clear which was the right drag coefficient to use in the rise velocity computation, considering that the bubbles in the experiment accumulated a fair amount of surfactants and the Reynolds number of the bubbles ranged over two decades (1-100). Two different velocities were computed for comparison, corresponding to the contaminated surface with a no slip boundary condition and to the clean surface with a stress-free interface with internal circulation cases. The rise velocity for these two limiting conditions[25] are given in Eqs. (1) and (2), respectively. These values were used for comparison with the rise velocity of the large bubbles, in the size range of the original experiments from which they were developed

$$Cd = \frac{24}{Re} \cdot \left(1 + \frac{1}{8} Re^{0.72}\right), \qquad V_z = \frac{d^2}{18 \cdot \nu_f \cdot \left(1 + \frac{1}{8} Re^{0.72}\right)} \cdot g, \tag{1}$$

$$Cd = \frac{11.1}{Re} \cdot Re^{-0.28}, \qquad V_z = \frac{4 \cdot d^2}{33.3 \cdot \nu_f \cdot Re^{-0.28}} g. \tag{2}$$

The non dimensional difference between the rise velocity of the bubbles in the turbulent flow and the velocity predicted for contaminated rigid bubbles in still fluid, Eq. (1), is

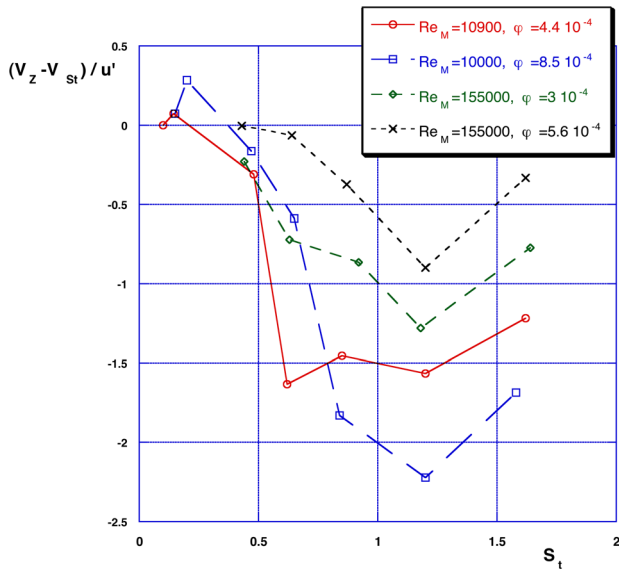

FIG. 11. (Color online) Rise velocity reduction for bubbles in the 400-1000 μm range.

shown in Figure 11. One can observe the presence of a minimum for values of Stokes number close to unity. The comparison of the turbulent bubble rise velocity with the two limiting cases of the drag coefficient is shown in Figure 12. In the lower curve, the rise velocity of bubbles is compared to the one predicted in still fluid for a clean, fully recirculating sphere that has the lowest drag coefficient, Eq. (2). In the upper one, the measurements are again compared against the velocity predicted for a bubble with a contaminated interface that behaves as a solid sphere due to the surfactants inhibiting any internal circulation, and has a higher drag coefficient, Eq. (1). It is worth noting that the conditions in the present experiment were closer to the fully contaminated, rigid surface than to the clean, recirculating sphere, and thus a very large reduction was obtained when the measurements were compared to the maximum rise velocity obtained for the clean spherical bubble. However, as both curves present negative values, one can claim unequivocally that there is a reduction of the rise velocity of the bubbles due to the turbulence, regardless of the uncertainty on the concentration of surfactants in the experiment.

For the case of the smallest bubbles, the experimental data from Detsch[26] were used for comparison. These were obtained for very small bubbles, using distilled, tap, and sea water. The values for tap and sea water were found to be almost identical and were used as a good approximation to the conditions in our experiments. In that paper, the values

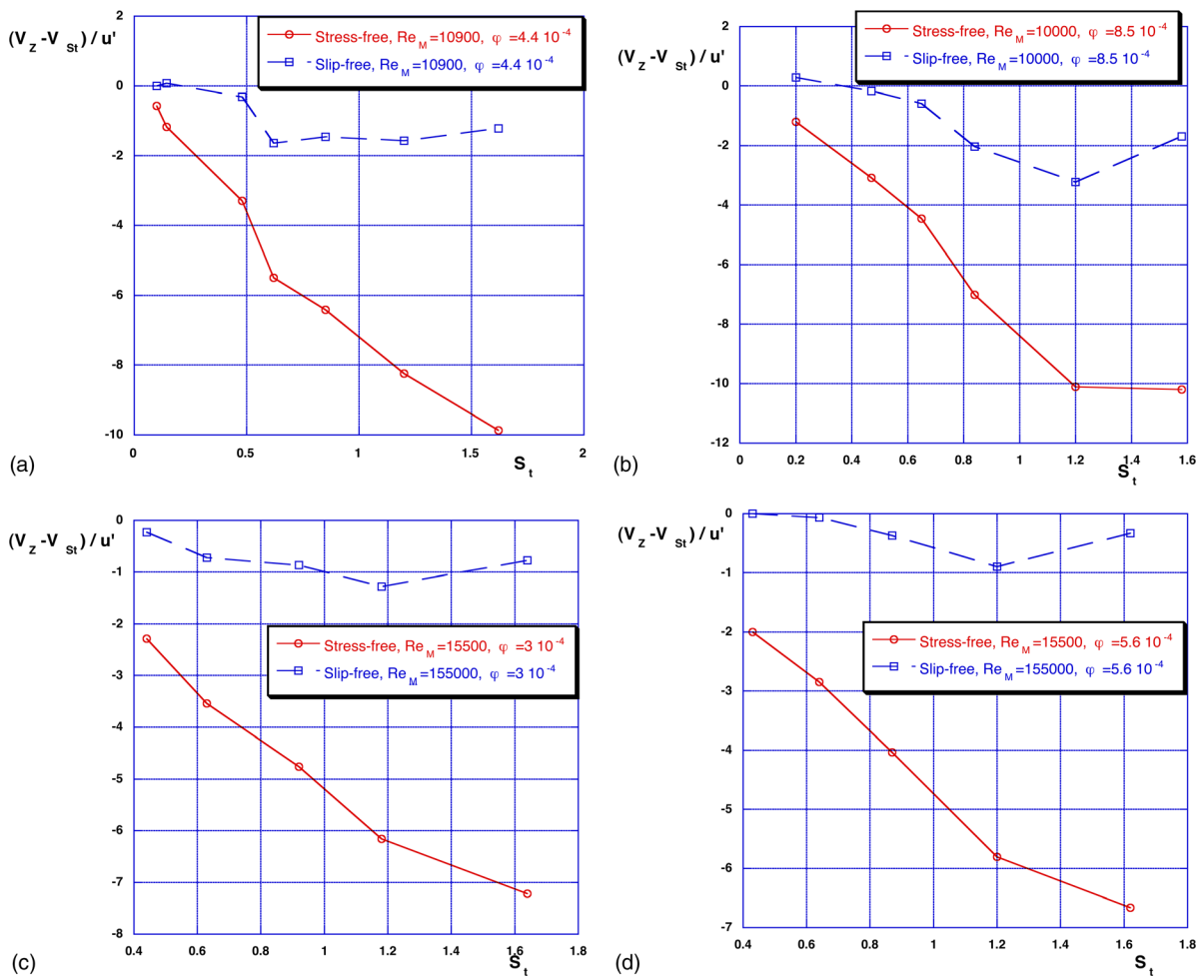

FIG. 12. (Color online) Rise velocity reduction as a function of the bubble Stokes number. Stress free, clean surface and internal circulation (Eq. (2)), and slip-free, contaminated surface with no internal circulation (Eq. (1)).

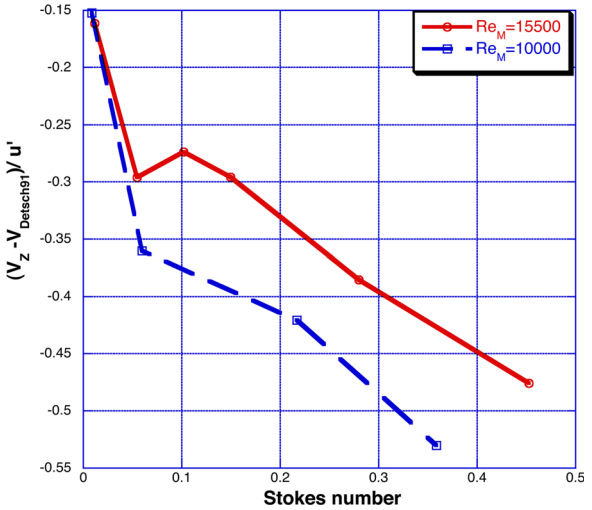

FIG. 13. (Color online) Rise velocity reduction for bubbles in the 50-400 μm range.

of rise velocity obtained for tap and sea water were fitted by a three term empirical law given in Eq. (3),

$$V_z = -4.71\,10^{-3} + 1.12\,10^{2} \cdot d + 1.42\,10^{4} \cdot d^2, \qquad (3)$$

where the velocity is given in meters per second and d is the bubble diameter in meters.

The values of the reduction in rise velocity of the smaller bubbles can be seen in Figure 13 and were found to be significant. When the reduction is non-dimensionalized with the root mean square of the fluctuating velocity of the carrier fluid, the results seem to collapse, in good agreement with the hypothesis that the rise velocity reduction is caused by the interaction of the bubbles with the turbulent structures and u′ is a measure of the level of turbulent kinetic energy present in this flow.

V. CONCLUSIONS

We have performed a series of experiments under well controlled conditions to understand the behavior of small air bubbles in a turbulent flow. Homogeneous isotropic decaying turbulent flow was created by a grid located at the entrance of the test section of a high Reynolds number horizontal water channel. The bubbles injected into the turbulent flow were allowed to interact with the turbulence for a large number of viscous relaxation times to ensure that the memory of the initial conditions was lost and their behavior was only a function of their diameter and the characteristics of the turbulence.

We used two different correlations found in the literature to compare our measurements of the vertical velocity of the bubbles against the rise velocity of bubbles of equal size in still fluid. The values from Detsch[26] were used for the smallest bubbles (50 – 400 μm), while the values from Maxworthy *et al.*[25] were used for the larger ones. The two correlations were found to give consistent values in the overlap region of validity.

The rise velocity of bubbles in a nearly homogeneous and isotropic turbulent flow is reduced with respect to the values measured in still fluid. This reduction was very significant, even for very small bubbles (in the 50 – 400 μm). The reduction in the rise velocity was maximum for bubbles with Stokes number of order unity. The Stokes number was computed using the Kolmogorov time scale of the turbulence, a choice consistent with previous studies in the literature. The r.m.s. of the turbulent velocity fluctuations was used to make the reduction of the rise velocity non dimensional. Thus, the curves obtained for different turbulence intensities were found to collapse to a certain extent.

The interaction of the bubbles with the turbulence in the carrier fluid leads to the formation of large inhomogeneities in the concentration field of the bubbles, in good agreement with previous numerical simulations.[4] Although this phenomenon has been described in heavy inertial particles,[5,6,29] the scaling for preferential concentration behaviour in bubbles had previously not been studied and experimentally confirmed. We found that the scale at which this accumulation due to the turbulent structures is more efficient is equal to 20 times the Kolmogorov scale of the turbulence. This is larger, although of the same order of magnitude, than the result in heavy particles. The difference in the value of the Reynolds numbers of the carrier flows, 10^5 vs. 6×10^5, was hypothesized to lead to a larger scale for the maximum of the turbulent dissipation spectrum where vorticity is most intense and therefore to be responsible for the increase in the bubble clusters.

[1]M. Maxey and J. Riley, "Equation of motion for a small rigid sphere in a nonuniform flow," Phys. Fluids **26**, 883 (1983).
[2]J. Magnaudet and I. Eames, "The motion of high Reynolds-number bubbles in inhomogeneous flows," Ann. Rev. Fluid Mech. **32**, 659 (2000).
[3]K. Tio, A. Liñán, J. Lasheras, and A. Gañán Calvo, "On the dynamics of buoyant and heavy particles in a periodic Stuart vortex flow," J. Fluid Mech. **254**, 671 (1993).
[4]L. Wang and M. Maxey, "The motion of microbubbles in a forced isotropic and homogeneous turbulence," Appl. Sci. Res. **51**, 291 (1993).
[5]L. Wang and M. Maxey, "Settling velocity and concentration distribution of heavy particles in homogeneous isotropic turbulence," J. Fluid Mech. **256**, 27 (1993).
[6]A. Aliseda, F. Hainaux, A. Cartellier, and J. Lasheras, "Effect of preferential concentration on the settling velocity of heavy particles in homogeneous isotropic turbulence," J. Fluid Mech. **468**, 77 (2002).
[7]P. Spelt and A. Biesheuvel, "On the motion of gas bubbles in homogeneous isotropic turbulence," J. Fluid Mech. **336**, 221 (1997).
[8]M. Maxey, B. Patel, E. Chang, and L. Wang, "Simulations of dispersed turbulent multiphase flow," Fluid Dyn. Res. **20**, 143 (1997).
[9]O. Druzhinin and E. Elghobashi, "Direct numerical simulations of bubble-laden turbulent flows using the two fluid formulation," Phys. Fluids **10**, 685–697 (1998).
[10]I. Mazzitelli, D. Lohse, and F. Toschi, "On the relevance of the lift force in bubbly turbulence," J. Fluid Mech. **488**, 283 (2003).
[11]G. Ruetsch and E. Meiburg, "2-way coupling in shear layers with dilute bubble concentrations," Phys. Fluids **6**, 2656 (1994).
[12]E. Climent and J. Magnaudet, "Dynamics of a two-dimensional upflowing mixing layer seeded with bubbles: Bubble dispersion and effect of two-way coupling," Phys. Fluids **18** 103304 (2006).
[13]E. Climent, M. Simonnet, and J. Magnaudet, "Preferential accumulation of bubbles in Couette-Taylor flow patterns," Phys. Fluids **19** 083301 (2007).
[14]M. Lance and J. Bataille, "Turbulence in the liquid phase of a uniform bubbly air-water flow," J. Fluid Mech. **222**, 95 (1991).
[15]T. Panidis and D. Papailiou, "The structure of two-phase turbulence in a rectangular channel: an experimental study," Int. J. Multiphase Flow **26**, 1369 (2000).
[16]G. Segre and A. Silberberg, "Behaviour of macroscopic rigid spheres in Pouiseuille flow," J. Fluid Mech. **14**, 115 (1962).
[17]P. Rightley and J. Lasheras, "Bubble dispersion and interphase coupling in a free shear flow," J. Fluid Mech. **412**, 21 (2000).

[18]G. Sridhar and J. Katz, "Drag and lift forces on microscopic bubbles entrained by a vortex," Phys. Fluids **7**, 389 (1995).
[19]E. Loth and M. Cebrzynski, "Modulation of shear-layer thickness due to large bubbles," Int. J. Multiphase Flow **21**, 919 (1995).
[20]V. Roig, C. Suzanne, and L. Masbernat, "Experimental investigation of a turbulent bubbly mixing layer," Int. J. Multiphase Flow **24**, 35 (1998).
[21]R. Poorte and A. Biesheuvel, "Experiments on the motion of gas bubbles in turbulence generated by an active grid," J. Fluid Mech. **461**, 127 (2002).
[22]W. Bachalo, "Experimental methods in multiphase flows," Int. J. Multiphase Flow **20**, 261 (1994).
[23]A. Aliseda, E. J. Hopfinger, J. C. Lasheras, D. M. Kremer, A. Berchielli, and E. K. Connolly, "Atomization of viscous and non-Newtonian liquids by a coaxial, high-speed gas jet. Experiments and droplet size modeling," Int. J. Multiphase Flow **34**, 161 (2008).
[24]A. Aliseda and J. Lasheras, "Effect of buoyancy on the dynamics of a turbulent boundary layer laden with microbubbles." J. Fluid Mech. **559**, 307 (2006).
[25]T. Maxworthy, C. Gnann, M. Kurten, and F. Durst, "Experiments on the rise of air bubbles in clean viscous liquids," J. Fluid Mech. **321**, 421 (1996).
[26]R. Detsch, "Small air bubbles in reagent grade water and seawater 1. Rise velocities of 20 to 1000 μm diameter bubbles," J. Geophys. Res. **96**, 8901, doi:10.1029/91JC00484 (1989).
[27]R. Clift, J. Grace, and M. Weber, *Bubbles, Drops and Particles* (Academic, New York, 1978).
[28]J. Eaton and J. Fessler, "Preferential concentration of particles by turbulence," Int. J. Multiphase Flow **20**, 169 (1994).
[29]K. Squires and J. Eaton, "Preferential concentration of particles by turbulence," Phys. Fluids **3**, 1169 (1991).